energies

MDPI

Article

Evaluation of the Factors Influencing Residual Oil Evolution after Alkali/Surfactant/Polymer Flooding in Daqing Oilfield

Chunlin Nie [1,2], Xiaolin Wu [3], Zhaowei Hou [2], Junjian Li [1,*] and Hanqiao Jiang [1]

[1] State Key Laboratory of Petroleum Resources and Prospecting, China University of Petroleum (Beijing), Beijing 102249, China; niechunlin@petrochina.com.cn (C.N.); jianghq@cup.edu.cn (H.J.)
[2] Exploration and Development Research Institute, Daqing Oilfield Co., Ltd., Daqing 163712, China; houzhw@petrochina.com.cn
[3] PetroChina Daqing Oilfield Co., Ltd., Daqing 163002, China; wuxldq@petrochina.com.cn
* Correspondence: junjian@126.com

Abstract: The alkali/surfactant/polymer (ASP) flood has long been considered to reduce residual oil saturation significantly after waterflood. This paper provides an experimental investigation of the factors (permeability, pore structure, ASP formula, injection volume, viscosity, and injection volume) that influence the evolution of residual oil after ASP flooding. ASP flood experiments were conducted on the cores drilled in Daqing field, and two-dimensional real-structure micromodels were constructed based on these cores. For the ASP core flood experiments, X-ray computed tomography imaging was used for the visualization of the residual oil evolution. For the ASP micromodel flood experiments, images of the residual oil distribution were obtained using a microscope with a 5× magnification objective. The results showed that as water saturation increased during the flood, the proportion of oil clusters decreased, and the proportion of oil droplets first increased and then decreased. For the cores with smaller pore throats and more complex pore structure, the residual oil became more scattered. In this case, the oil clusters became smaller, and oil droplets became easier to retain. An increased injection rate improved the emulsification, resulting in more residual oil in small pores getting replaced. Increasing the viscosity by increasing the polymer concentration improved the sweep efficiency, mainly because residual oil in large pore throats was displaced, but had a negative impact on emulsification. Increasing the viscosity of the injection fluid was shown to have a negative impact on improving the oil recovery ratio, because the mobilization of residual oil in smaller pores was greatly impacted by emulsification. The effect of increasing injection volume on improving recovery was more pronounced for cores with lower permeability.

Keywords: ASP flood; residual oil evolution; microfluidic

Citation: Nie, C.; Wu, X.; Hou, Z.; Li, J.; Jiang, H. Evaluation of the Factors Influencing Residual Oil Evolution after Alkali/Surfactant/Polymer Flooding in Daqing Oilfield. *Energies* **2022**, *15*, 1048. https://doi.org/10.3390/en15031048

Academic Editor: Rouhi Farajzadeh

Received: 16 December 2021
Accepted: 21 January 2022
Published: 30 January 2022

1. Introduction

Daqing Oilfield is experiencing an ultrahigh water cut, and now is the first oilfield in the world that has implemented field-scale chemical flooding projects [1–3]. The ordinary tertiary displacement method (polymer-only or surfactant-only flooding) cannot provide sufficient improvement in oil recovery. To further displace the remaining oil in Daqing, more effective methods are needed. Through laboratory tests, alkali/surfactant/polymer (ASP) flooding has shown to effectively produce the remaining oil in high water content rock core. However, there are great differences in development effects between ASP flooding development blocks and single wells. Especially after the development object changes to worse-developed class II oil reservoirs, there is a certain gap between the development effects of some blocks and the expectations. In order to clarify the factors that influence the effect difference change from the mechanism and further improve the development effect of ASP flooding, it is necessary to carry out in-depth research on the evolution law and factors influencing microresidual oil in ASP flooding so as to guide the targeted improvement of the performance of the oil displacement system and formulate

development countermeasures. ASP flooding has long been studied in labs through core flooding experiments [4–7]. By studying the pore structures of the cores, Zhang [8] found that the pore structure of different sedimentary microfacies reservoirs had a significant impact on oil displacement efficiency and that the pore structure was one of the main controlling factors determining residual oil patterns. Hou [9] used CT technology to study the occurrence state of microresidual oil in water drive. Wu [10] carried out a microsimulation model displacement experiment on real pore throat fabrication with a cast sheet to study the micromechanism of remaining oil after water flooding of ternary composite system. Zhang [11] applied the microdisplacement experiment and quantitative analysis method of residual oil in an artificial sandstone sample formation system to core samples with different pore structures to obtain and quantitatively analyze the distribution of residual oil under different water injection multiples and pore structure characteristics in core pores. Fang [12] used CT to quantitatively analyze the micropores of real cores and studied the relationship between different oil droplet sizes and oil content after ASP flooding. Li et al. [13] studied the effect of pore structure characteristics on microresidual oil during water flooding with a CT scanning water flooding experiment. Wang [14] quantitatively characterized the micropore structure of natural cores by CT and studied the variation law of micropore structure parameters of water flooding and ASP flooding. However, there are still problems with quantitative analysis, which mainly focuses on saturation. The complexity and variability of pore structure and occurrence of remaining oil clusters make it difficult to quantitatively analyze the distribution characteristics of microresidual oil. In research methods on microresidual oil, because of the low resolution (for most methods, above 10 μm), the residual oil cluster is the smallest research unit, so it is impossible to analyze the production process of microresidual oil in each pore unit before and after ASP flooding and give clear guidance on the lower limit of residual oil production under different pore throat structure conditions.

In this present study, we studied the factors influencing residual oil evolution after alkali/surfactant/polymer flooding in Daqing Oilfield. Microresidual oil research on ASP flooding was carried out through natural cores, and systematic research on factors influencing residual oil was carried out in combination with a microfluidic experiment. We focused on the effect of injection rate, injection fluid viscosity, and injection fluid volume on improvement in oil recovery via ASP flooding. The results were compared for different pore structures and sizes.

2. Methods and Materials

2.1. Materials

Core samples: ASP core flood experiments were conducted on a series of cores drilled from the class II oil layer of the Sartu formation in Daqing Oilfield. The lowest permeability among these cores was 320 md, and the highest was 1793 md, with the porosity varying from 24.4 to 30.1%.

According to the statistical results of pore throats of cast thin sections, the samples shown in Table 1 were divided into three types based on their pore structures: large pore and large throat with medium heterogeneity, medium pore and medium throat with strong heterogeneity, and small pore and small throat with weak heterogeneity. The average ratios of pore radius to throat radius of the three model types were 2.11, 2.20, and 1.96, respectively. The degree of heterogeneity was ordered as follows: medium pore and medium throat strong heterogeneity (#7) > large pore and large throat medium heterogeneity (#1) > small pore and small throat weak heterogeneity (#64). The difference of pore/throat radius in the medium-pore, small-throat model was the largest, and the difference of pore/throat-radius in the small-pore, small-throat model was the smallest.

Table 1. Properties of cores used for ASP flood experiments.

Number	Permeability Classification	Experiment Number	Porosity (%)	Permeability (mD)	Diameter (mm)	Length (mm)
#1	High	1	30.1	1793	8	50
#5	Medium	2-1	28.1	925	8	50
#7	Medium	2-2	28.3	1088	8	50
#9	Low	3	27.8	545	8	50
#64	Low	4	25.6	320.0	8	50

Micromodel: the micromodel (or microfluidic chip) used in the ASP flood experiments was a two-dimensional chip fabricated with glass. We constructed three micromodels (Table 2) based on the extracted pore structure and surface characteristics from microCT images of cores #1, #7, and #9 in Table 1 so that real rock properties and morphological features such as porosity, permeability, and pore and grain size distribution were transferred into the 2D microfluidic chips. The micromodel measurement was 30 mm × 20 mm, with permeability between 0.3 and 2 μm^2.

Table 2. Samples and Parameters used in the microfluidic experiments.

Model	Experiment Number	Displacement Rate (μL/min)	System Viscosity (mPa·s)	System Consumption (PV)	Experimental Purpose
#1 Large pore, large throat, medium heterogeneity	1	0.01	30	0.5	different injection velocity
	2	0.05	30	0.5	
	3	0.1	30	0.5	
	4	0.05	40	0.5	different system viscosity
	5	0.05	50	0.5	
	6	0.05	30	0.3	different system dosage
	7	0.05	30	0.7	
#2 Medium pore, medium throat, strong heterogeneity	1	0.01	30	0.5	different injection velocity
	2	0.05	30	0.5	
	3	0.1	30	0.5	
	4	0.05	40	0.5	different system viscosity
	5	0.05	50	0.5	
	6	0.05	30	0.3	different system dosage
	7	0.05	30	0.7	
#3 Small hole, small throat, weak heterogeneity	1	0.01	30	0.5	different injection velocity
	2	0.05	30	0.5	
	3	0.1	30	0.5	
	4	0.05	40	0.5	different system viscosity
	5	0.05	50	0.5	
	6	0.05	30	0.3	different system dosage
	7	0.05	30	0.7	

Fluid: The properties of the Daqing crude oil used herein were as follows: density, 0.8629 g/mL; freezing point, 29 °C: sulfur content, 0.11%; nitrogen content, 1586 ppm; acid value, 0.08; nickel and vanadium contents, 4.36 ppm and 0.13 ppm, respectively. It is a low-sulfur, medium-paraffin-based crude oil. Into Daqing Oilfield crude oil was dissolved 5 wt% diiodomethane (to improve the contrast of scanning image), and the viscosity was 10MPa·s at 45 °C. The injection water was produced water.

Chemical reagent: petroleum sulfonate surfactant; analytical-grade sodium carbonate alkali; medium (12–16 million) partially hydrolyzed polypropylene amide polymer.

The microfluidic experimental scheme is shown below:

2.2. Experimental Procedure

2.2.1. ASP Core Flood Experiment

The core flood procedure is summarized as follows:

1. Dry core scanning: pore structures were obtained by CT scanning of original dry core;
2. Saturated water: the core with was saturated with formation water;
3. Saturated oil: the core was saturated with crude oil added with 5 wt% diiodomethane oil at the rate of 0.01 mL/min. After the pressure stabilized, initial saturation was calculated from the CT images;
4. Water flood: 3 PV formation water was injected at 0.01 mL/min, and the CT scan was continued;
5. ASP flood: 0.5 PV of petroleum sulfonate/new active agent 0.3% + alkali 1.2% + intermediate polymer (viscosity is 30 mPa·s at 45 °C) was injected at 0.01 mL/min, and the CT scan was continued.

2.2.2. ASP Micromodel Flood Experiment

The micromodel flood procedure is summarized as follows:

1. Water flood: at the speed of 0.05 ul/min, the micromodel was flooded with water until stabilized, and the final water cut was observed to be 98%;
2. ASP flooding: 0.3/0.5/0.7 PV of petroleum sulfonate/new active agent 0.3% + alkali 1.2% + intermediate polymer, (viscosity is 30/40/50 mPa·s at 45 °C, respectively) was injected at 0.01/0.05/0.1 mL/min, respectively;
3. Water flood: water was injected until a stabilized recovery and a stabilized pressure drop profile were obtained. Here we observed a water cut of 98%.
4. A total of 18 micromodel displacement experiments were completed and recorded.

2.3. Discussion

2.3.1. Residual Oil Classification

According to the characteristic parameters of 3D microresidual oil, a quantitative classification standard of 3D microresidual oil was established. Based on the analysis of a large number of previous experimental results and following Li [15], microresidual oil was divided into five categories—membrane, droplet, column, porous, and cluster, ordered by increasing levels of residual oil mobilization—and the corresponding occurrence characteristics and geneses were defined. The types of the residual oil patterns were classified based on four parameters: the pore throat number, the morphological factor, the contact ratio, and the Euler number.

The average pore and throat radii were calculated using the AVIZO software and classified using the maximum sphere algorithm.

2.3.2. Maximum Sphere Algorithm

In the maximum sphere algorithm, any point in the pore space is taken as the benchmark. The maximum inscribed sphere is located where the center is just tangent to the boundary of the rock skeleton. After all the spheres are located, the spheres contained in other inscribed spheres are removed as redundant spheres, and the remaining spheres constitute the largest sphere set and can describe the pore space without redundancy. The clustering algorithm is used to classify and combine the largest ball set to identify pores and throats. Pores are represented by larger balls, while throats between pores are represented by a series of smaller balls. The algorithm proceeds as follows:

1. At each pixel on the path, place a sphere with a small radius around it, and expand the radius of the sphere until the circumference contacts the rock skeleton. In this way, the largest sphere that can be placed in the pore space such that the center of the sphere is on the path is obtained.
2. Delete all contained spheres and divide the remaining overlapping spheres into two categories: primary and secondary. For intersecting spheres, that with larger radius is

the primary sphere, and that with the smaller radius is the secondary sphere. In the figure, pink is the main sphere and blue is the auxiliary sphere.

3. Check whether there is a locally largest master sphere on the path (excluding the two endpoints). If so, mark the center of the master sphere as a pore node. As shown in Figure 1, the blue star in Figure 1 marks the new nodes.

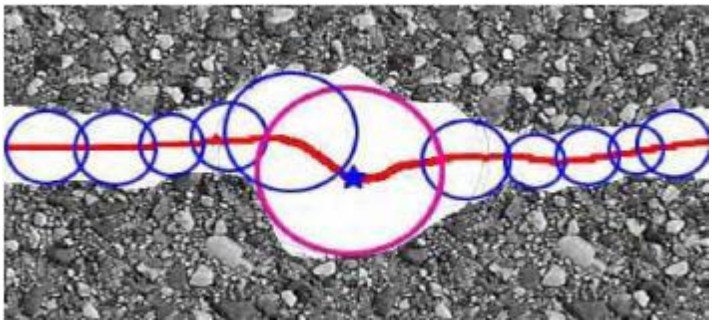

Figure 1. Searching nodes with coordination number 2 by the graph maximum sphere method.

The central axis after path correction and node correction is shown in Figure 2. Each curve segment corresponds to a throat, each node corresponds to the center position of the hole, and the number of curve segments connected by the node corresponds to the coordination number of the hole.

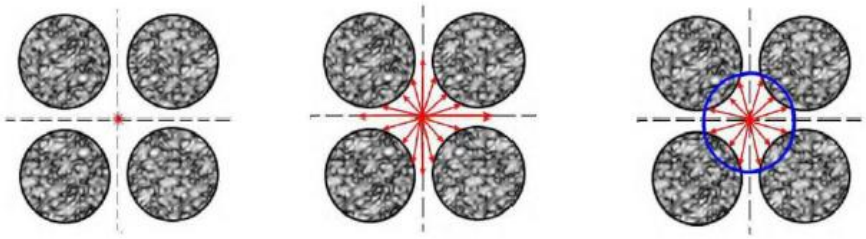

(**a**) (**b**) (**c**)

Figure 2. (**a**) Pore diagram; (**b**) schematic diagram of pore length measurement; (**c**) schematic diagram of calculated pore length.

After the central axis of pore space is obtained, pore throat structure segmentation can be realized by the "ray method" and "maximum class spacing method".

The "ray method" refers to taking the pore center as the origin, sending out a ray at a certain angle, extending the ray until it stops growing after reaching the rock particles, recording the length of all ray segments, and finally obtaining the dataset composed of the length value marking the pore radius.

For the dataset obtained by the "ray method", the "maximum class spacing method" mentioned above was adopted, and the threshold, K, was set to minimize the variance in the two separate data groups and maximize the variance between groups. The average value of the smaller set of data was the equivalent pore radius.

2.3.3. Residual Oil Identification

The images obtained from the experiment were analyzed using commercial software. First, the rock skeleton and pores were separated. On this basis, the oil and water in the pores were separated, and the types of remaining oil were quantitatively divided according to the classification standard of remaining oil so as to provide the basis for later statistical analysis.

In this study, water was extracted by the watershed threshold method (Figure 3), and oil was extracted by the single point window threshold method to achieve the separation

of rock, oil, and water. As 5 wt% diiodomethane was added to the experimental displacement crude oil, the oil in the scanning image was in bright white, which could be well distinguished from the rock skeleton and oil.

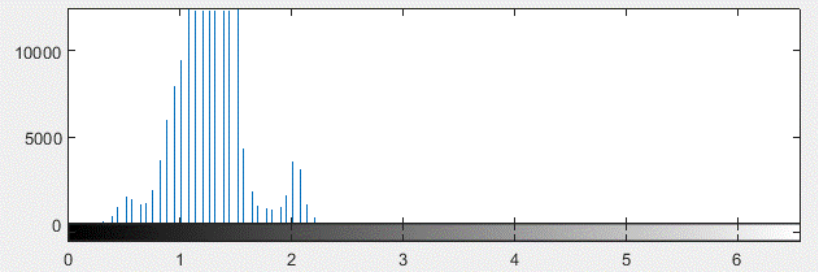

Figure 3. Watershed threshold method.

The procedure of the watershed threshold method used was as follows:

The first step was to make histogram statistics on the gray value of each image. The abscissa was the gray value of the image, the number of groups was usually set to 256, and the ordinate was the gray value frequency within the gray value range of each group. The water in the image was bright white, and the corresponding gray value was the highest. Therefore, the first peak on the right of the histogram was the water, and the higher peak in the middle was the gray value corresponding to the rock skeleton. There was an obvious watershed between the two peaks, and the abscissa corresponding to the watershed was the threshold for segmenting the skeleton and water.

The second step was to accurately obtain the position of the watershed. In this study, the difference method was used for this purpose. It was noted that the frequency of gray values on both sides of the watershed first decreased and then increased, that is, the difference of the frequency on the left side of the watershed was less than 0, and the difference of the frequency on the right side of the watershed was greater than 0.

In the third step, after the threshold was determined, all the gray values greater than the threshold were extracted, and the image was optimized to obtain the oil part. Figure 4 below is an example.

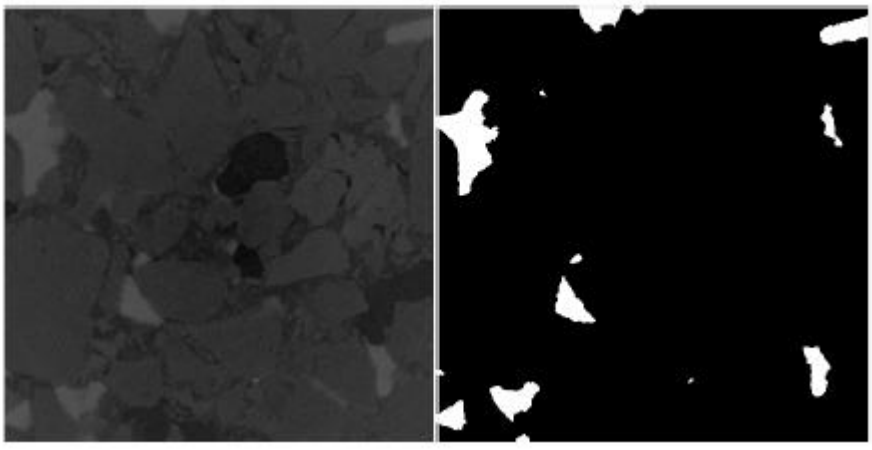

Figure 4. Example of image extraction.

Because the gray values of rock skeleton and oil were relatively close, the watershed threshold method could not distinguish oil and rock skeleton well, and the binary method was needed to distinguish them. The traditional binarization method, the Otsu algorithm, also known as the "maximum class spacing method", realizes binarization by setting a global threshold. Its idea is to determine the threshold according to the ratio of the variance of the two groups of average values (intergroup variance) to the variance of each group (intragroup variance). Note that the number of pixels, average value, and variance

are represented by N, μ, σ, Subscripts 1 and 2 represent the two groups of pixels after binarization, subscript T indicates all pixels. Thus, the variance within the group was:

$$\sigma_W^2 = \frac{N_1}{N_T}\sigma_1^2 + \frac{N_2}{N_T}\sigma_2^2 \tag{1}$$

The intergroup variance was:

$$\sigma_B^2 = \frac{N_1}{N_T}(\mu_1 - \mu_T)^2 + \frac{N_2}{N_T}(\mu_2 - \mu_T)^2 \tag{2}$$

The selection of threshold k maximized the subordinate ratio; the formula was as follows:

$$\frac{\sigma_B^2(k)}{\sigma_\pi^2(k)} = max\left(\frac{\sigma_B^2}{\sigma_W^2}\right) \tag{3}$$

Subscript W means within the group variance and B means between the group variance. Traditional methods have a poor binarization effect for pictures with uneven exposure, as shown in the Figure 5. As shown in Figure 5, the traditional global threshold binarization method has poor effect.

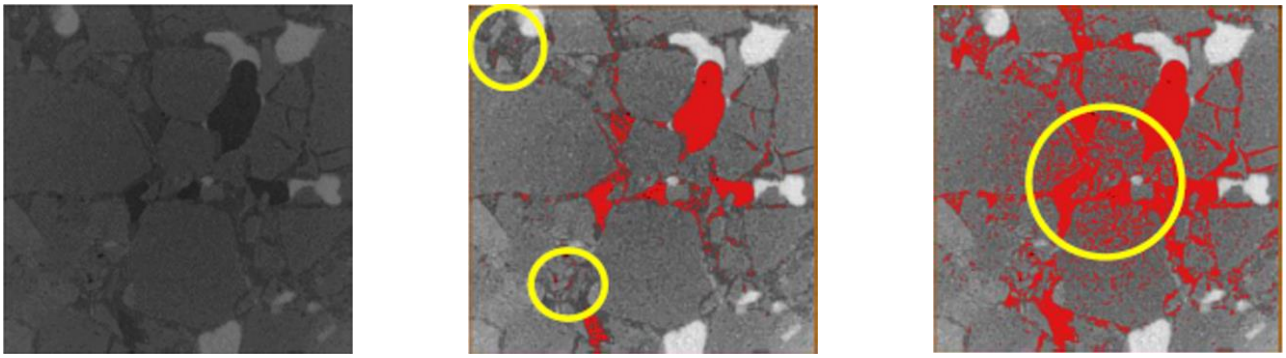

(**a**) (**b**) (**c**)

Figure 5. The traditional global threshold binarization method has a poor effect. (**a**) Original image; (**b**) Effect drawing of threshold binarization method and (**c**) Traditional business software (Avizo) processing results.

The single point window threshold method opens a window at each pixel of the whole picture on the basis of the Otsu algorithm and then calculates a threshold for the window with the Otsu algorithm.

The procedure as used was as follows. In the first step, the extracted water was set as the gray value of typical rock. At this time, as shown in Figure 6, the image had only two parts—oil and rock skeleton.

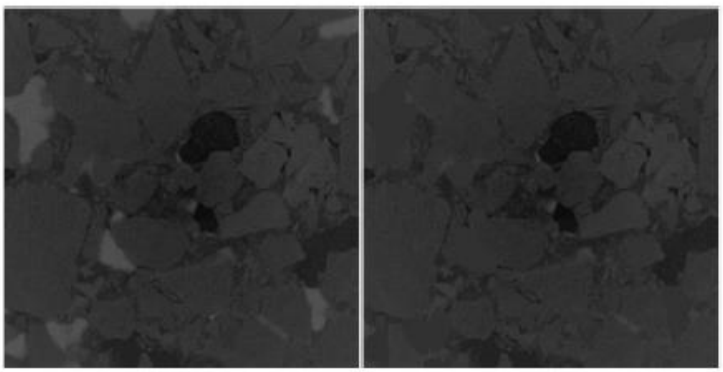

Figure 6. Replace the gray value of water with the gray value of typical rock.

The second step was to open a window at each pixel (x, y) of the obtained image containing only rock skeleton and oil and calculate a threshold T (x, y) for the window with Otsu algorithm. When the gray value I (x, y) < T (x, y) at the pixel (x, y), the point was oil; otherwise, it was skeleton. Figure 7 shows the gray value of water being replaced with the gray value of typical rock.

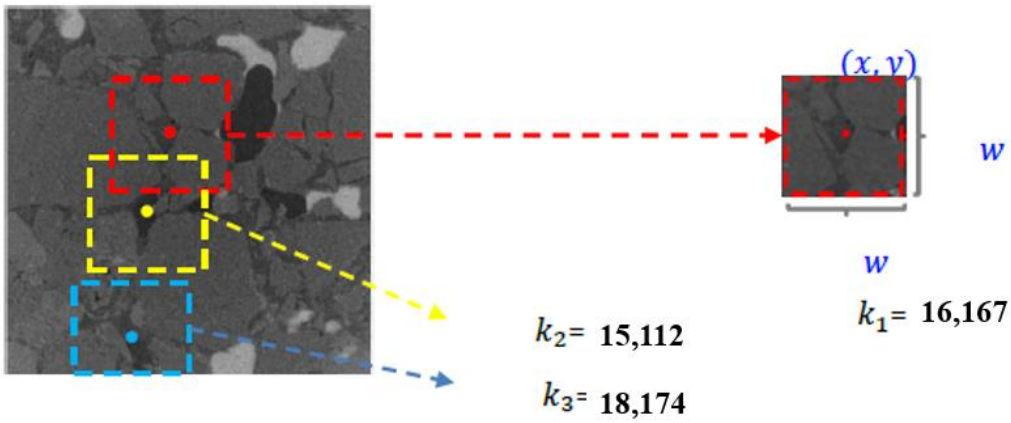

Figure 7. Schematic diagram of the single point window threshold method.

3. Study on the Evolution Law of Microresidual Oil in Compound Flooding

We observed that most of the residual oil in cluster form was displaced in the ASP core flood; the amount of residual oil in droplet form first increased and then decreased; and other types of residual oil form stayed unchanged. The residual oil in smaller pores is displaced, resulting in higher oil recovery.

3.1. The Evolution Characteristics of Residual Oil after ASP Flooding

The relative content under different microresidual oil volumes is shown in Figure 8. The distribution of different residual oil types in high-permeability cores (#1) after ASP flooding and changes in cluster residual oil with different permeability before and after ASP flooding are shown in Figure 9. The cluster residual oil production in high- permeability cores, medium- permeability cores, and low-permeability cores (#1) after ASP flooding are different as shown in Figure 10.

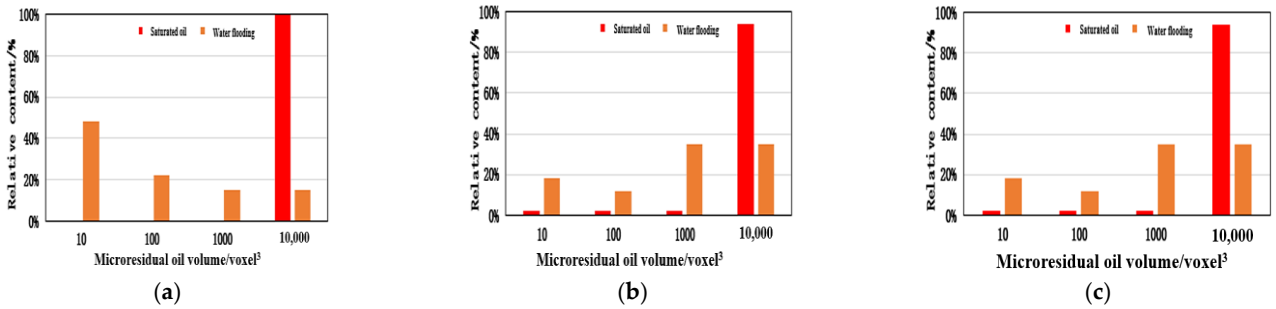

Figure 8. Relative content under different microresidual oil volumes. (**a**) Relative content under different microresidual oil volumes for low-permeability cores. (**b**) Relative content under different microresidual oil volumes for medium-permeability cores. (**c**) Relative content under different microresidual oil volumes for high-permeability cores.

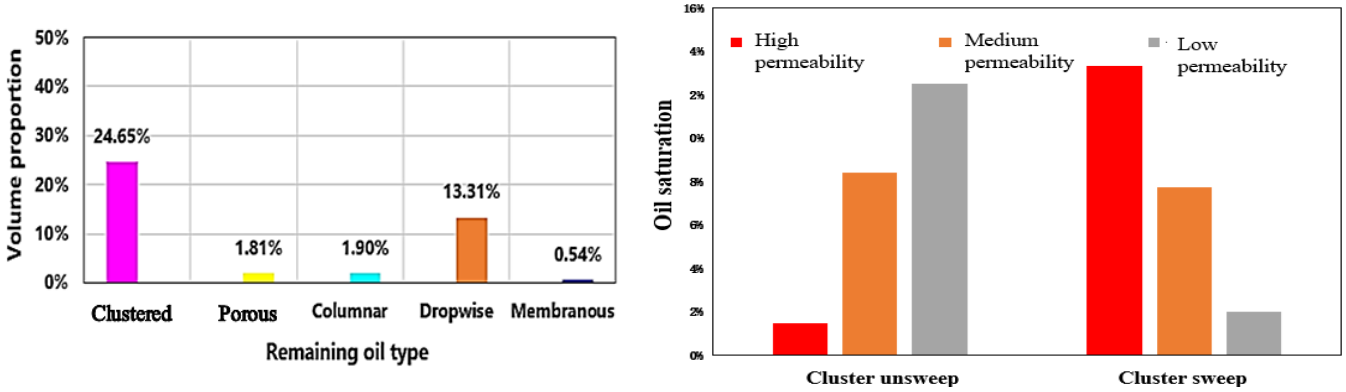

Figure 9. (**a**) Distribution of different residual oil types in high-permeability cores (#1) after ASP flooding; (**b**) changes in cluster residual oil with different permeability before and after ASP flooding.

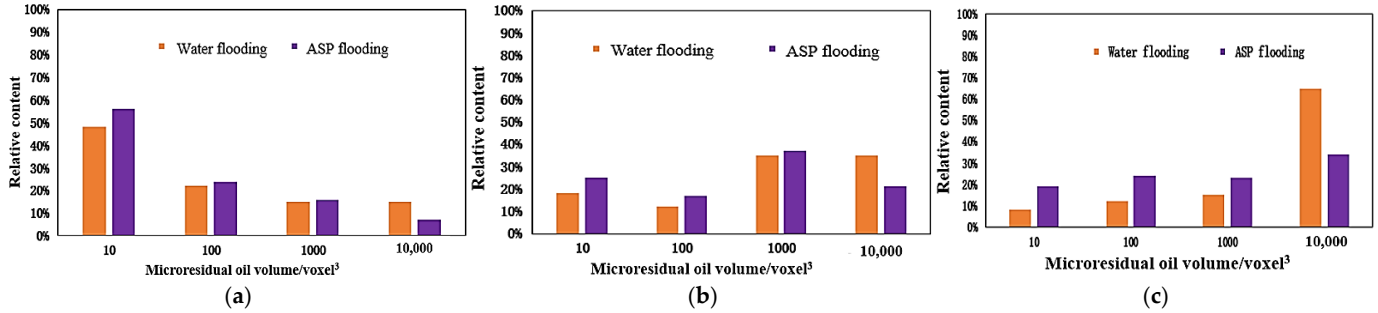

Figure 10. Cluster residual oil production in (**a**) high-permeability cores after water flooding and ASP flooding, (**b**) medium-permeability cores after water flooding and ASP flooding, and (**c**) low-permeability cores after water flooding and ASP flooding.

As shown in Figures 8 and 9, the less permeable the core became, the more residual oil in cluster form was displaced, and the more residual oil in droplet form was retained. For high-permeability cores, the ASP flood mainly improved recovery of the residual oil in cluster form, while for low-permeability cores, it helped displace the immobilized oil clusters in the water flood. For high-permeability cores, after ASP flood, the proportion of large oil clusters decreased significantly, and the proportion of small clusters increased, indicating that the residual oil in high permeability core became more scattered after ASP flooding. For low-permeability cores, the proportion of large oil clusters decreased compared with that for high-permeability cores. According to the relative content under different microresidual oil volumes in the figure below, the proportion of cluster residual oil with volume greater than 10,000 voxel^3 increased, indicating the residual oil was not scattered after ASP flood.

3.2. Effect of Pore Throat Characteristics on the Evolution of Residual Oil after ASP Flood

The pore diameter of different oil phase volumes and pore volumes under water flooding and ASP flooding is shown in Figure 11a, the relative content of different microresidual oil volumes under water flooding and ASP flooding in a large-pore, medium-throat core (#9) is shown in Figure 11b. The pore diameter of different oil phase volumes and pore volumes under water flooding and ASP flooding is shown in Figure 12a, the relative content of different microresidual oil volumes under water flooding and ASP flooding in a large pore, small throat core (#64) is shown in Figure 12b. From the distribution of pore and throat radius, the pore radius and throat radius of the two cores were close, but the pore/throat ratio was quite different. If the pore/throat ratio of core #64 was greater than that of the #9 core, they were defined as a large-hole, small-throat core and a large-hole, medium-throat core, respectively. More oil in large pores and medium size throats was

displaced, but the shear effect was insignificant, the emulsification degree was low, and the degree of accumulation of the remaining oil was high. After large pore medium throat ASP flooding, 40–90 um pores were obviously effectively utilized. The volume of clusters of residual oil was mainly 10,000 voxel^3, accounting for 41% of all residual oil volume. The residual oil in large-pore, medium-throat cores was less scattered than that in large-pore, small-throat cores. For the pore structures with large pores and small throats, oil in smaller pores was displaced after ASP flooding. The residual oil in 10 μm pores was effectively displaced, while oil in 5 μm pores was not significantly displaced. The volume of clusters of residual oil was mainly 10 voxel^3, accounting for 56% of all residual oil volume.

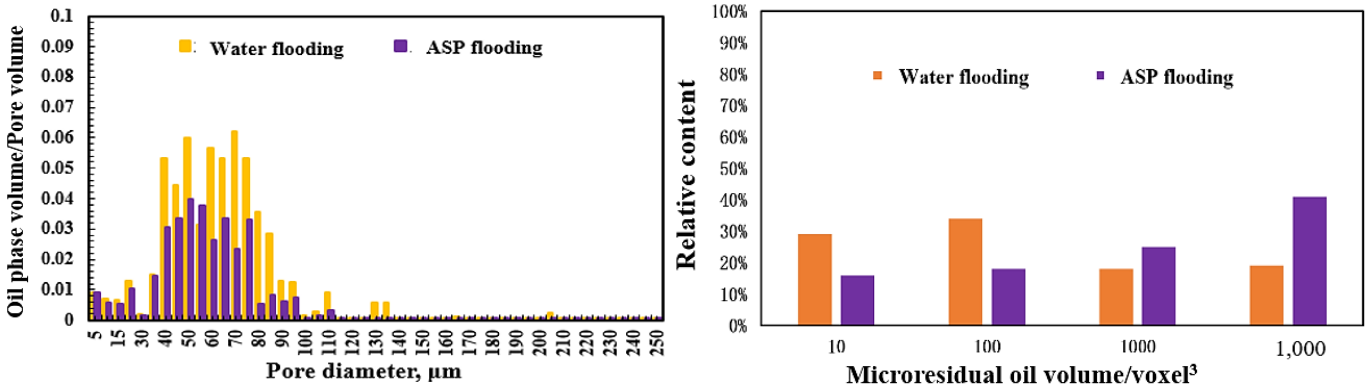

(**a**) (**b**)

Figure 11. Pore production and distribution of various residual oil in a large-pore, medium-throat core (#9) after ASP flooding. (**a**) The pore diameter of different oil phase volumes and pore volumes under water flooding and ASP flooding, (**b**) The relative content of different microresidual oil volumes under water flooding and ASP flooding.

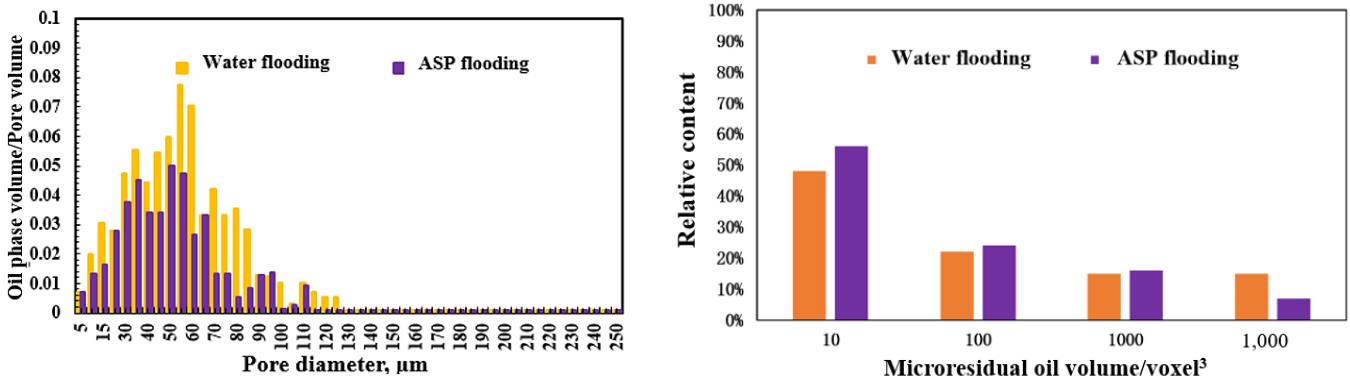

(**a**) (**b**)

Figure 12. Pore production and distribution of various remaining oil in a large-pore, small-throat core (#64) after ASP flooding. (**a**) The pore diameter of different oil phase volumes and pore volumes under water flooding and ASP flooding, (**b**) The relative content of different microresidual oil volumes under water flooding and ASP flooding.

3.3. Study on Microresidual Oil Composition Characteristics and the Evolution Law of Different ASP Flooding Systems

As shown in Figure 13, the residual oil was mainly in cluster and droplet form after sulfonate ASP flood. There was some residual oil in porous, columnar, and film form, but it accounted for a proportion of no more than 2%. After ASP flooding using the new formula, the residual oil types were like those after using the oil formula, but the proportion of the residual oil in droplet form was larger than that in cluster form. As shown in Figure 14, for the sulfonate system, because of the insufficient emulsifying ability, most of the residual oil in clusters was larger than 1000 voxel^3. The emulsifying ability of the new formula was

significantly better than that of the sulfonate system. The cluster-form residual oil after ASP flooding was mainly smaller than 100 voxel^3, and residual oil became scattered after ASP flooding using the new formula.

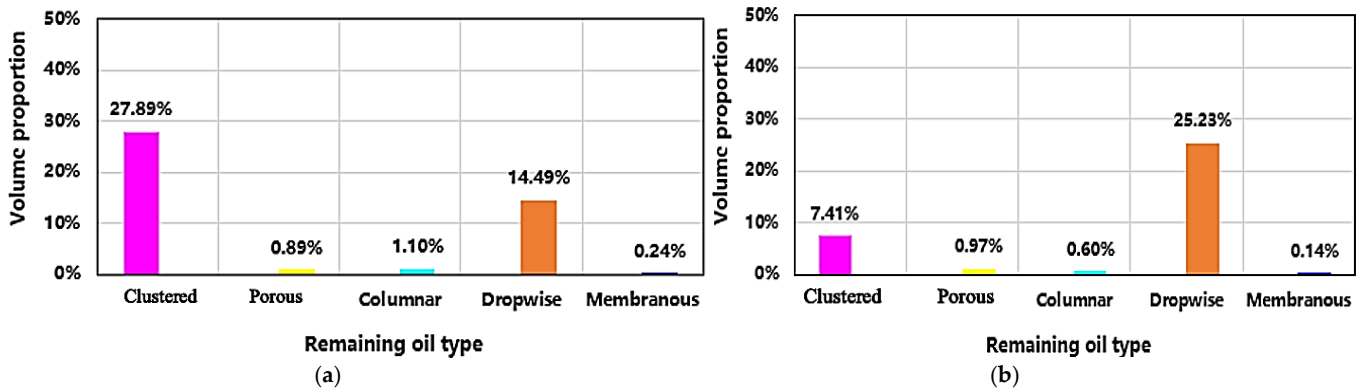

Figure 13. Distribution of residual oil in the sulfonate system and the new system. (**a**) Distribution of residual oil in the sulfonate system, (**b**) Distribution of residual oil in the new formula.

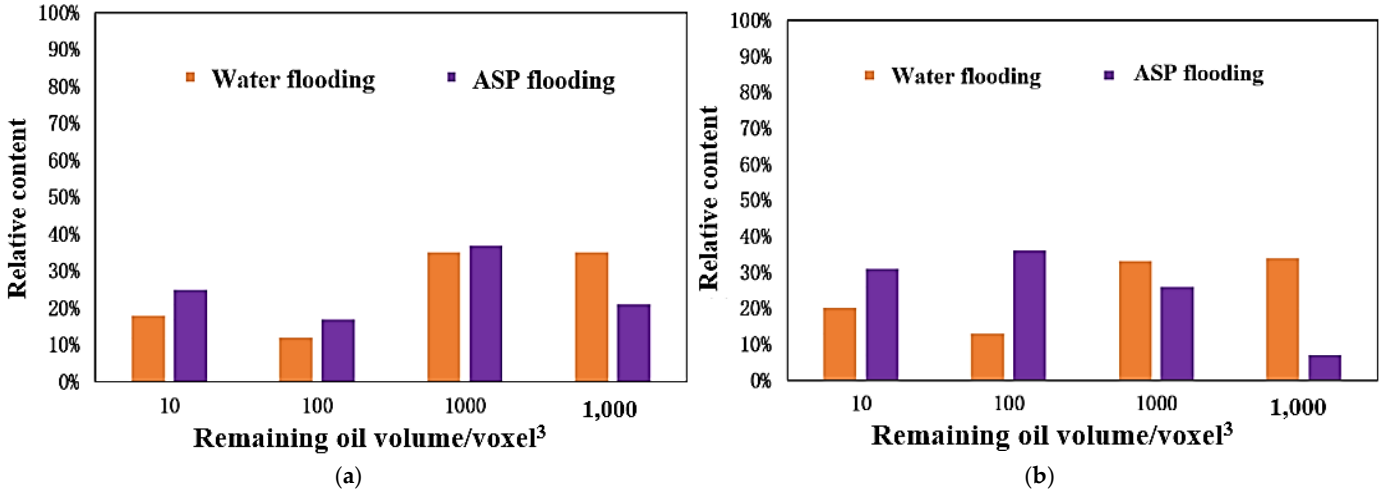

Figure 14. Cluster residual oil production after ASP flooding with the sulfonate system and the new formula. (**a**) Cluster residual oil production after ASP flooding with the sulfonate system, (**b**) Cluster residual oil production after ASP flooding with the new formula.

4. Influencing Factors of Residual Oil

4.1. Effect of Injection Rate on Residual Oil

The effect of injection rate on residual oil evolution was studied on the three different models presented in Table 2, and the results all showed improved oil recovery under higher injection rates. Comparisons with the results in different pore sizes show that this effect was observed to be more pronounced in pores with smaller throat radius (5–20 μm) and that more oil was displaced with increased injection rates. This was because the higher the injection rate was, the stronger the emulsification was. As shown in Figure 15, emulsification consequently had a significant effect in the improving the mobility of the residual oil in the small pores. Moreover, if the displacement rate was lower than 0.05 μL/min, it was difficult to displace the remaining oil in pore throats of less than 10 μm because of higher resistance in smaller pores. When the displacement rate was less than 0.05 μL /min, the residual oil bound in pore throat radii of less than 10 um was hardly displaced.

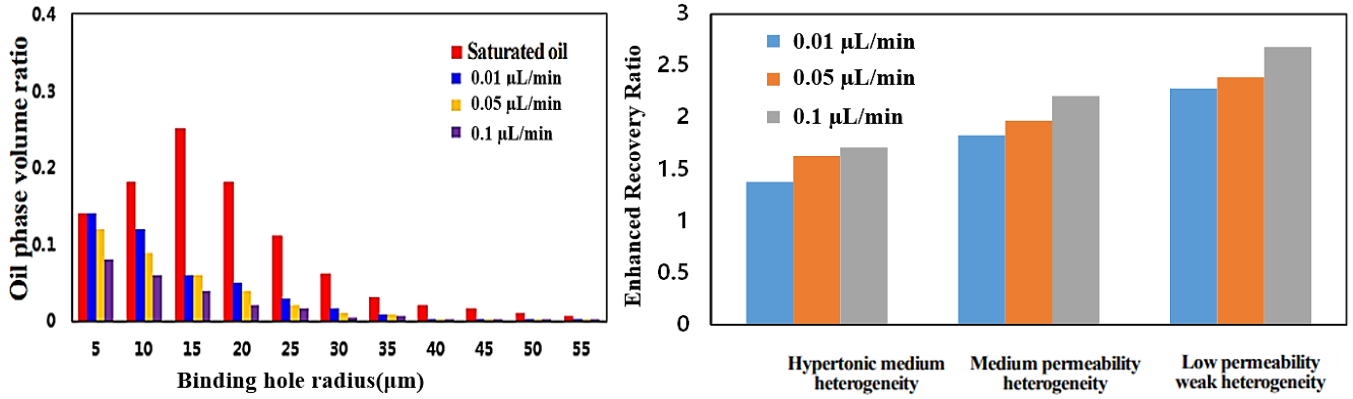

Figure 15. Producing porosity and displacement effects at different injection rates.

4.2. Effect of the Viscosity of Injection Fluid on the Evolution of Residual Oil

Figure 16 presents the effect of changing injection fluid viscosity on residual oil evolution. Unlike Section 4.1, increased viscosity was shown to have a negative impact on improving oil recovery ratio in all three of models tested. This was the result of increasing viscosity having a negative impact on emulsification. The polymer improved the mobility ratio to expand the sweep efficiency, which was mainly characterized by the evolution of cluster-type remaining oil. On the other hand, porous and dripping residual oil mainly reflected microscopic oil's displacement efficiency; in such cases, ASP flooding improved oil recovery through emulsification, stripping porous remaining oil and changing the status of residual oil. This was confirmed because as viscosity increased, more oil in pore throat radii larger than 15 μm was displaced.

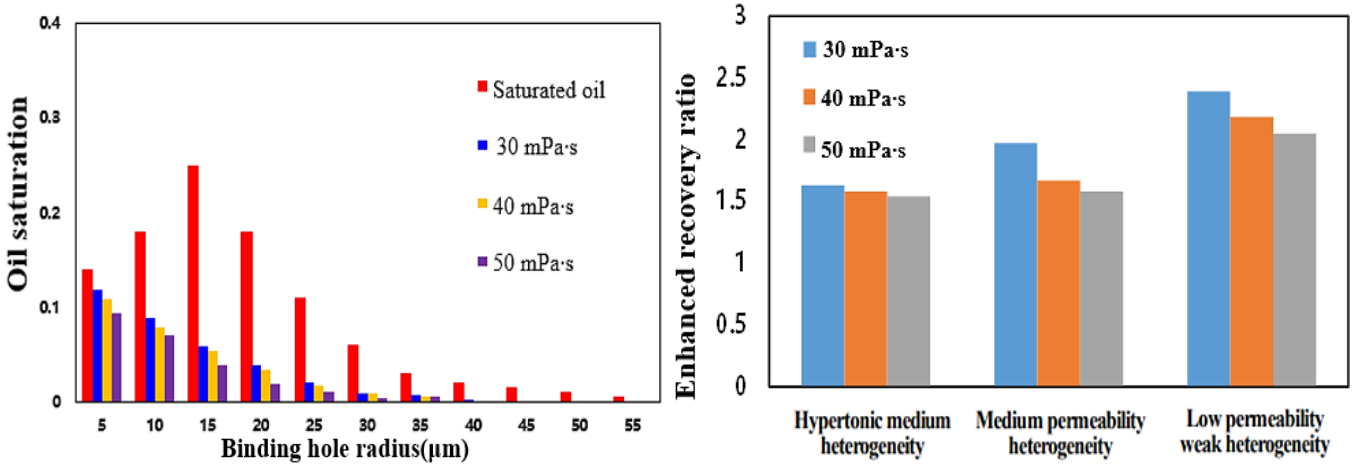

Figure 16. Producing porosity and displacement effect with different injection viscosity.

4.3. Effect of Injection Volume on Residual Oil Evolution

Figure 17 presents the effect of changing injection fluid volume on residual oil evolution. With increasing of injection volume, the oil displacement efficiency change was negligible, while enhancement in emulsification led to the improvement of recovery. As injection volume increased, the droplet-form residual oil in the small pores was increased, the emulsification was enhanced, more oil in the 5–10 μm pore throat radius was displaced, and the recovery was increased by 31.69%, indicating that for small pores, the injection volume should be increased to improve recovery. For models with different pore throat structures, the emulsifying ability increased with increasing injection volume. Emulsification has a strong effect to help displace residual oil in pore throats with radii of 5–10 μm; the lower the permeability, the more a significant change in recovery was observed by increasing the injection volume. In other words, with a continuous increase in injection volume,

the emulsification was enhanced, and the final recovery was increased. However, in the 5–10 μm pores, the main factor affecting the recovery was the pore size, not emulsification.

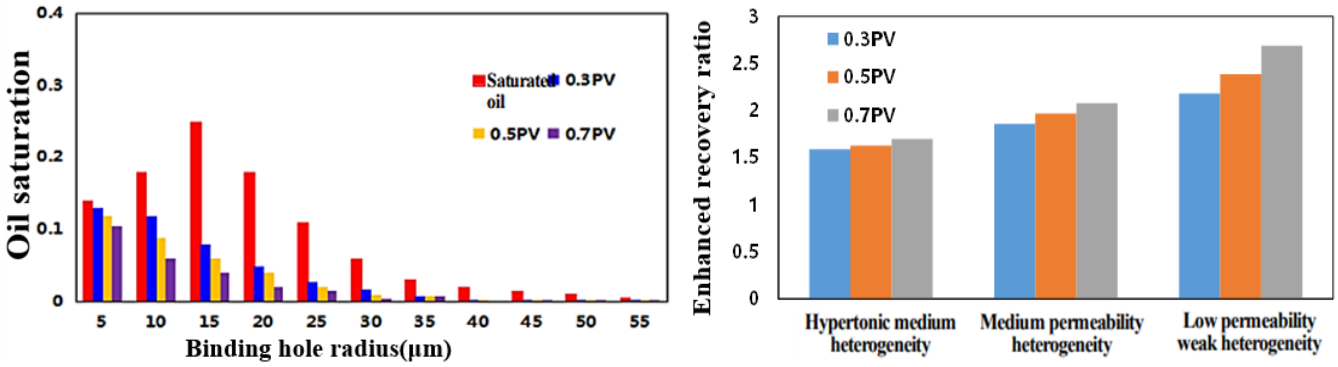

Figure 17. Producing porosity and displacement effects with different injection volume.

5. Conclusions

1. As water saturation increased in water flood, the amount of residual oil in cluster decreased, and the amount of residual oil in droplet form first increased and then decreased; for the cores with smaller pore throats and more complex pore structures, the residual oil became more scattered, and the volume of the residual clusters became smaller. Compared with flooding using the old formula, ASP flooding with the new surfactant formula resulted in smaller volumes and more scattered distributions of residual oil.
2. Increasing the injection rate enhanced the emulsification effect and thus improved the mobilization of the residual oil in smaller pores. Increasing viscosity helped displace the residual oil in large pores. The lower the permeability, the more increasing the injection volume led to a significant impact on recovery improvement.
3. The experimental work was focused on the class II reservoir of the Sartu formation in Daqing Oilfield. The evolution of residual oil after ASP flooding in a greater variety of formations and pore structures will be studied in our future work.

Author Contributions: Conceptualization, X.W., Z.H. and H.J.; methodology, C.N. and J.L.; investigation, C.N.; writing—original draft preparation, C.N.; writing—review and editing, J.L.; supervision, H.J., X.W. and Z.H.; funding acquisition, X.W. and Z.H. All authors have read and agreed to the published version of the manuscript.

Funding: National Science and Technology major project "Daqing Changyuan extrahigh water cut oilfield EOR demonstration project" (2016zx05054).

Institutional Review Board Statement: Not applicable.

Informed Consent Statement: Not applicable.

Data Availability Statement: Not applicable.

Conflicts of Interest: The authors declare no conflict of interest.

References

1. Sun, L.; Wu, X.; Zhou, W.; Li, X.; Han, P. Technologies of enhancing oil recovery by chemical flooding in Daqing Oilfield, NE China. *Pet. Explor. Dev.* **2018**, *45*, 673–684. [CrossRef]
2. Li, Y.; Wang, F.; Wu, J.; Yang, Z.; Chen, G.; Zong, L.; Peng, S. Current Status and Prospects of ASP Flooding in Daqing Oil Fields. Available online: https://onepetro.org/SPEIOR/proceedings-abstract/08IOR/All-08IOR/SPE-114343-MS/144443 (accessed on 10 December 2021).
3. Cheng, J.; Xu, D.; Bai, W. Commercial test of ASP Flooding in Daqing Oil Field. Available online: https://onepetro.org/SPEADIP/proceedings-abstract/08ADIP/All-08ADIP/SPE-117824-MS/145439 (accessed on 10 December 2021).
4. Zhang, Y.; Huang, S.; Dong, M. Determining the Most Profitable ASP Flood Strategy for Enhanced Oil Recovery. *J. Can. Pet. Technol.* **2005**, 44. [CrossRef]

5. Panthi, K.; Sharma, H.; Mohan, K.K. ASP flood of a viscous oil in a carbonate rock. *Fuel* **2016**, *164*, 18–27. [CrossRef]
6. Rahul, S.; Ramgopal, U.; Pankaj, T. Impact of natural surfactant, polymer and silica nanoparticles to enhance heavy crude oil recovery. *Energy Fuels* **2019**, *33*, 4225–4236.
7. Rahul, S.; Ramgopal, U.; Pankaj, T. Influence of emulsification, interfacial tension, wettability alteration and saponification on residual oil recovery by alkali flooding. *JIEC* **2018**, *59*, 286–296.
8. Zhang, Y. Study on micro pore structure characteristics of sandstone reservoir in Xingnan oilfield, Daqing. Ph.D. Thesis, Northeast Petroleum University, Daqing, China, 2011.
9. Hou, J.; Qiu, M.; Lu, N.; Qu, Y.; Li, F.; Meng, X.; Shi, X. Characterization of residual oil microdistribution at pore scale using computerized tomography. *Acta Pet. Sin.* **2014**, *35*, 319–325.
10. Wu, C.; Hou, J.; Zhao, F.; Zhang, F.; Hao, H.; Liu, G. Micro mechanism of remaining oil after water flooding in ternary composite system. *Oil Gas Geol. Recovery. Factor* **2015**, *22*, 84–88.
11. Zhang, Q. Study on micro residual oil in sandstone reservoir based on digital core. Master's Thesis, China University of Petroleum (East China), Qingdao, China, 2016.
12. Fang, Y. Study on micro residual oil distribution characteristics of class I block in Chaoyanggou Oilfield. Master's Thesis, Northeast Petroleum University, Daqing, China, 2018.
13. Li, J.; Jiang, H.; Wang, C.; Zhao, Y.; Gao, Y.; Pei, Y.; Wang, C.; Dong, H. Pore-scale investigation of microscopic remaining oil variation characteristics in water-wet sandstone using CT scanning. *J. Nat. Gas Sci. Eng.* **2017**, *48*, 35–36. [CrossRef]
14. Wang, X.; Shen, Z.; Zhang, D.; Hu, S.; Zhang, B.; Zhang, X. Micro pore structure characteristics after ASP flooding based on full diameter core CT scanning technology. *Daqing Pet. Geol. Dev.* **2019**, *38*, 81–86.
15. Li, J.; Liu, Y.; Gao, Y.; Cheng, B.; Meng, F.; Xu, H. Effect of micro pore throat structure heterogeneity on remaining oil distribution. *Pet. Explor. Dev.* **2018**, *45*, 1043–1052. [CrossRef]